2002 HST Calibration Workshop
Space Telescope Science Institute, 2002
S. Arribas, A. Koekemoer, and B. Whitmore, eds.

STIS Flux Calibration

R. Bohlin

Space Telescope Science Institute, 3700 San Martin Drive, Baltimore, MD 21218

Abstract. The low dispersion STIS spectrophotometric flux calibration must account for all instrumental non-linearities and all changes in sensitivity with time and temperature. An empirical algorithm for CCD Charge Transfer Efficiency (CTE) is presented along with the wavelength dependent sensitivity changes. Precise STIS spectrophotometry includes corrections for CTE losses as large as 20% for faint signals and low sky, for MAMA non-linearities of $\sim 2\%$, and for loss in system throughput that currently reaches a maximum $\sim 15\%$ at 1625 Å with an average loss of more than 10% for G140L spectra on the FUV-MAMA. Newly available LTE and NLTE models from I. Hubeny's TLUSTY code are compared to the old flux distributions for the Koester/Finley LTE models of the four primary flux standards. The uncertainty in the corrections and in the flux standards are all small enough, so that flux distributions relative to 5500 Å in the V-band can be measured in the photometric 52×2 arcsec slit to a precision of $\sim 1\%$ over much of the 1150–10,000 Å STIS wavelength coverage. The NLTE model flux distributions are probably correct within $\sim$1% to 2.5 μ in the IR; and a model for the total uncertainty is presented.

1. Introduction

The SNAP (SuperNova/Acceleration Probe) mission to determine the dark energy equation of state parameters has motivated attempts to improve the precision of spectrophotometric standards to an accuracy of $\sim 1\%$ in the relative flux. In order to achieve the prime science goals, the SNAP program requires $\sim 1\%$ accuracy in the relative flux calibration over its 0.4–2 μ wavelength range. The *HST* primary standard stars used for the absolute flux calibration of STIS and NICMOS are directly relevant to the SNAP program.

In simple terms, the sensitivity of a spectrometer as a function of wavelength is used to measure the flux F of an observed science target or a secondary stellar flux standard by

$$F(\lambda) = C(\lambda)/S(\lambda) \quad , \tag{1}$$

where C is the observed count rate. To determine the sensitivity S, the most straightforward method is to observe a standard star with a known flux distribution $F_{\rm std}$

$$S = C_{\rm std}/F_{\rm std} \quad . \tag{2}$$

The best primary stellar flux standards from 0.1–3 μ are the set of four unreddened, pure hydrogen white dwarf (WD) stars G191B2B, GD153, GD71, and HZ43 (Bohlin 2000), while STIS secondary standards are presented by Bohlin, Dickinson, & Calzetti (2001). The temperature and gravity of the primary standards are determined from fits to the Balmer line profiles (e.g., Finley, Koester, & Basri 1997); and model atmosphere calculations determine the relative flux distributions (e.g., Barstow et al. 2001). Precise V-band photometry relative to Vega (Landolt 1992 & 1999, private comm.) sets the absolute flux scale of these four primary standards. The uncertainty in the absolute Vega flux distribution of Hayes (1985) combined with uncertainties in the normalization to the Landolt V magnitudes is

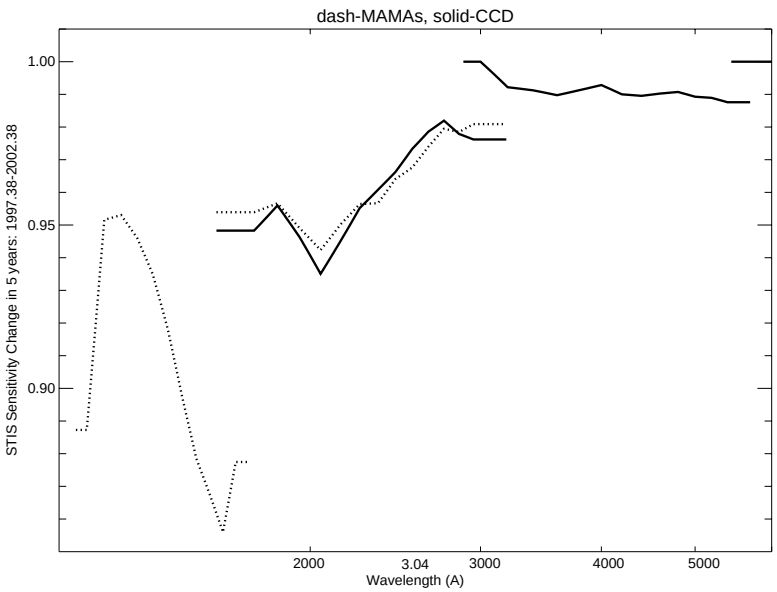

Figure 1. Change of sensitivity for the five low dispersion modes after five years of on-orbit operations: dotted lines—MAMA modes G140L and G230L, solid lines—CCD modes G230LB, G430L, and G750L corrected for CTE losses. All of the G750L sensitivity changes are assumed to be due to CTE loss.

$\sim 2\%$ at V, while the uncertainties in C(λ) relative to 5500 Å in the V-band are discussed in Section 2. Uncertainties in the calculated model flux distributions relative to 5500 Å are quantified in Section 3; and Section 4 has examples of actual uncertainties achieved in the measured STIS flux distributions of secondary flux standards.

2. Uncertainties in Measured Count Rates

The count rate C in Eq. 1–2 is for an observation with all of the instrumental signatures removed. These signatures include flat fielding, background removal, stray light, flagging of artifacts, fringing, operational changes, wavelength calibration, temperature effects, changes of sensitivity with time, and non-linear response of the detector. Because the effect of a slowly varying flat field in the dispersion direction is accounted in the sensitivity S calibration, the only benefit of a flat field calibration is the removal of the pixel-to-pixel sensitivity fluctuations, as long as the spectrum is always located at the same location on the detector. Precise background subtraction is important for the faintest stars and is complicated by geocoronal emission lines of Ly-α at 1216 Å and of OI at 1300 Å in the case of *HST*. For STIS spectra in the wide 52×2 photometric slit, stray light from the wings of the PSF fills in absorption lines. Beyond $\sim$ 6620 Å, fringing due to reflective interference in the CCD substrate becomes increasingly important as the sensitivity drops; and at 1 μ the fringing correction limits the repeatability to $\sim 1\%$, even for bright stars. In addition to the absence of atmospheric effects, observations from space generally benefit from the constancy of operational modes. In the case of STIS, the same wavelength hits close to the same pixel on the detector, year after year, so that slow temporal changes can be easily tracked. However, two STIS low dispersion modes have had major adjustments: the G140L default aperture moved from 3 arcsec above detector center to 3 arcsec below, while for the CCD modes, a new aperture at row 900 is available and reduces CTE losses by a factor of 5. Precise wavelength calibration is important in wavelength regions with steep sensitivity gradients. For the G140L mode on the FUV-MAMA there is a temperature dependence of the sensitivity

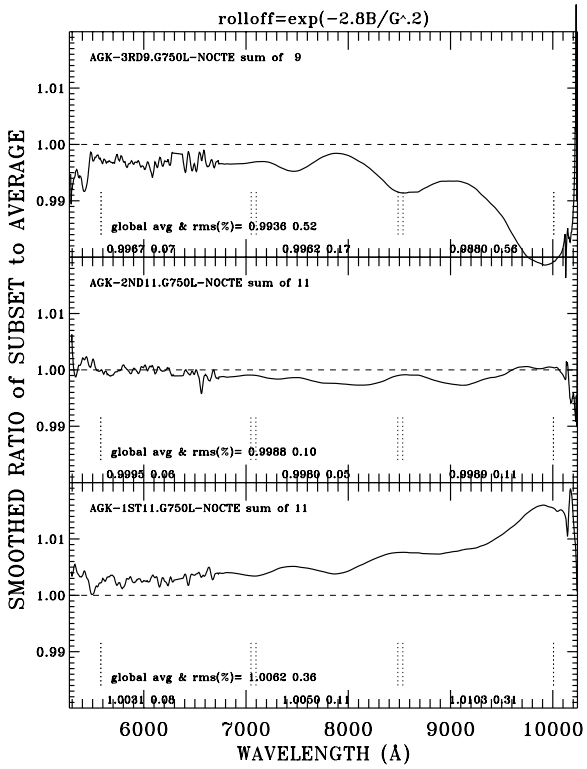

Figure 2. Ratios of the first (bottom), second (middle), and most recent third (top) to the average of all 31 observations of the bright CCD monitor star AGK+81D266 with NO correction for any change in sensitivity with time or for any CTE losses. The increasing effect of CTE losses with time are evident from the ratios > 1 in the bottom panel and < 1 in the top panel. There are small deviations from unity at the shorter wavelengths where the signal peaks at $\sim 40,000$ electrons and larger deviations as the signal drops continuously to ~ 1000 electrons at 1 μ. The increasing magnitude of the non-linearity at lower counting levels is a signature of CTE losses.

of 0.3%/C. The two most important limitations on the photometric precision of the STIS count rate corrections are: a) the observed scatter about the mean changes of the sensitivity with time and b) the uncertainty in the non-linear correction for CTE losses (see below).

The change in sensitivity as a function of wavelength and time has been reported by Bohlin (1999) and by Stys, Walborn, & Sahu (2002). Figure 1 shows the wavelength dependence of the sensitivity loss after five years in orbit for the five low dispersion STIS modes. Within a mode, the changes are continuous functions of wavelength; and the two modes, G230L on the NUV-MAMA and G230LB on the CCD, show the same changes to within $\sim 0.5\%$. The four discontinuous jumps from one mode to the next may be the result of blaze angle shifts in the first order gratings that are caused by shrinkage of the epoxy substrate of the replica grating rulings, as suggested by Bowers (this volume, p. 127) for the echelle modes.

Figure 2 illustrates the effects of Charge Transfer Efficiency (CTE) losses for the G750L mode. The monitoring observations of AGK+81D266 are divided into three epochs and compared to the average spectrum of all 31 observations of AGK+81D266 since launch. While the ratio of the middle third is near unity, the early 11 observations in the lower panel are higher than the average; and the 9 spectra obtained since 2001 July in the top

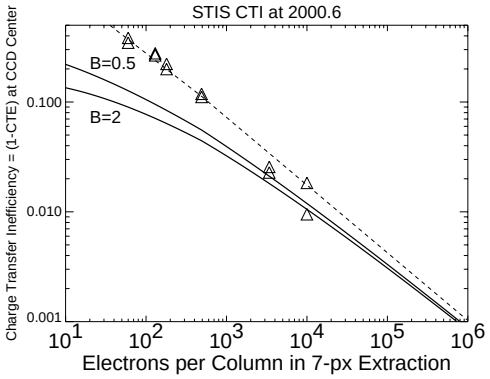

Figure 3. CTI(G,2000.6) at 2000.6, i.e. 3.44 years after launch at the center of the CCD. The abscissa is G, the total gross electrons recorded in the default 7-px high extraction box. The dashed line is a fit to the measurements (triangles) of Kimble (2001, private comm.) at 3.17 and 3.71 years after launch and is relevant to an image with zero background from a single readout of the CCD. The measurements have been divided by small amounts, 0.92 and 1.08 at 3.17 and 3.71 years, respectively, to correct the data points to the mean time of 3.44 years, so that the scatter within the pairs of points at each of the six electron levels is indicative of the uncertainty. Heavy solid lines: The CTI for background levels of 0.5 and 2 electron/px that are typical of gain 1.

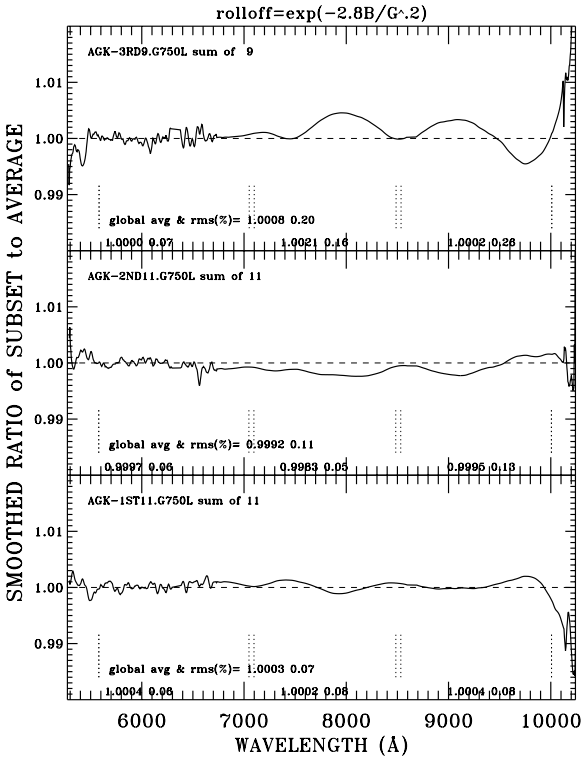

Figure 4. As in Figure 2 AFTER correction for CTE losses per Equation 1 and Figure 3. Residuals exceed 0.5% only for the last 100 Å of wavelength coverage beyond 10,100 Å.

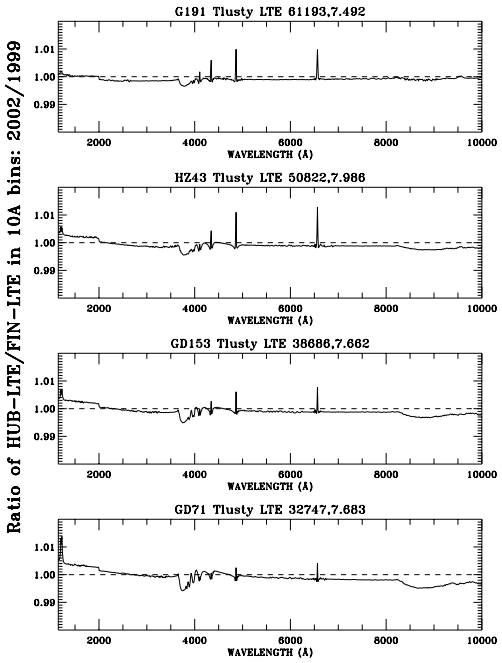

Figure 5. Ratios of Hubeny to Koester-Finley pure hydrogen models in LTE for the temperature and gravities indicated in each of the four panel titles. Differences approach 1% only in the 10 Å bin at the center of H-α and H-β for the two hottest stars. Compare with Fig. 1 of Bohlin (2000), which makes the same comparison before the TLUSTY code upgrades.

panel are below unity everywhere. The assumption that the behavior observed in Figure 2 is attributed entirely to CTE losses and not to optical sensitivity degradation is justified by the trend toward unity, i.e. no loss, at long wavelengths in Figure 1 and by the trend to larger losses toward longer wavelengths in Figure 2. CTE losses increase as the G750L signal decreases toward longer wavelengths. The triangles in Figure 3 illustrate the measured CTE losses at a mean date of 2000.6, 3.4 years after launch, for a mean background level of zero (R. Kimble 2001, private comm.). The heavy solid lines are the modeled losses at sky background levels of 0.5 and 2 electrons per pixel and are a best compromise correction for the AGK+81D266 data and for some short exposure observations of LDS749B and G191B2B (Bohlin 2002). The zero background fit to the data triangles in Figure 3 is the dashed line CTI(G, $t = 2000.6$), while the preliminary Charge Transfer Inefficiency $CTI = (1 - CTE)$ at time t in decimal years and rolloff for sky background B is

$$\begin{aligned} CTI(B,G,t) &= CTI(G,t)e^{-2.2(B/G)^{0.20}} \\ &= CTI(G,2000.6)\{(t-2000.6)0.242+1\}e^{-2.2(B/G)^{0.20}} \quad , \end{aligned} \tag{3}$$

where G is the gross signal in electrons in the seven pixel extraction height and where the CTI is assumed to linearly increase from zero at the 1997.16 launch date. The CTI increases linearly with the number of CCD rows from the readout amp, while the dashed line, CTI(G,2000.6), in Figure 3 is for the center of the CCD at row 512. The constants 2.2 and 0.20 in Equation 1 produce the best fit correction to the deviations from unity in Figure 2; and the ratios for these corrected observations of AGK+81D266 are illustrated in Figure 4, where the deviations from unity are $< 0.5\%$ below 1 μ.

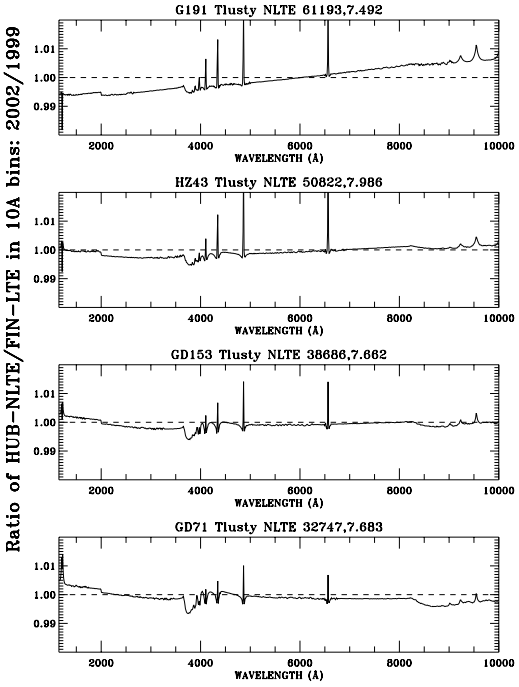

Figure 6. As in Figure 5, except with Hubeny NLTE models in the numerator. Differences approach 2% only in the 10 Å bin at the center of H-α and H-β for the two hottest stars. Compare with Fig. 2 of Bohlin (2000), which makes the same comparison before the TLUSTY code upgrades.

3. Uncertainties in the Model Flux Distributions

The model $T_{\rm eff}$ and $\log g$ are determined by fitting the observed Balmer line profiles (e.g. Finley, Koester, & Basri 1997). These fits have an internal consistency that implies an uncertainty of much less than 1% in the shape of model flux distributions from 0.1 to 3 μ. Since Bohlin (2000) reported inconsistencies between LTE calculations with the same temperature and gravity for the simplest pure hydrogen case, the model atmosphere codes have been upgraded (Barstow et al. 2001). Figure 5 demonstrates agreement within one percent in the optical between the new Hubeny and old Koester models for the four primary standards, even in the 10 Å band at the Balmer line centers. Furthermore, the Hubeny NLTE model line profiles agree with the Koester/Finley profiles to 2% at line center, as shown in Figure 6. Therefore, the Hubeny NLTE models are adopted as the best estimates of the true stellar flux distributions, because the physics is more realistic and because the Balmer line profiles are in agreement with the models and observations used by Finley to derive the temperature and gravity. The model flux distributions are placed on an absolute flux scale by normalizing to the V band magnitudes measured by Landolt with a precision of a few milli-magnitudes (Bohlin 2000). In the top panel for the hottest star G191B2B, the difference in the continuum slope starts to be evident and becomes larger in the IR.

In the IR, Figure 7 illustrates differences between the LTE and NLTE models of up to 4% at 3 μ for the hottest star. The NLTE model for G191B2B resolves the discrepancy (BDC 2001) between the standard star flux ratio and the measured NICMOS flux ratio for G191B2B/P330E, as shown in Figure 8. On average, the data points lie closest to the heavy solid line for the NLTE model.

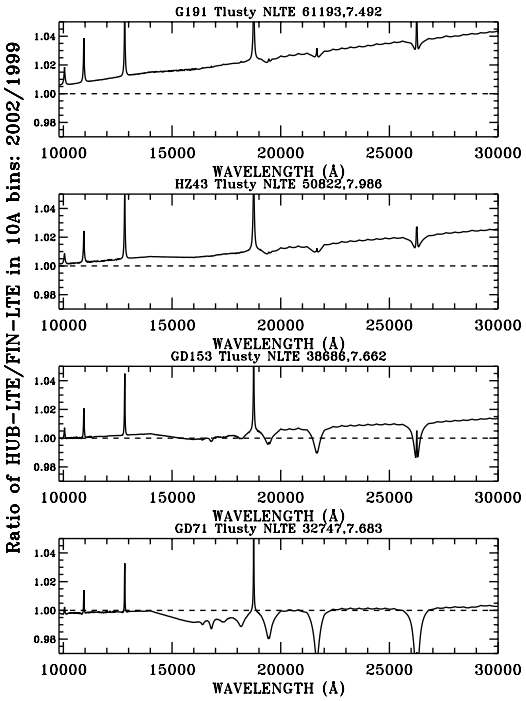

Figure 7. As in Figure 6, except that the wavelength range is 1–3 μ. There is a difference between LTE and NLTE of $\sim 4\%$ at 3 μ for the hottest star G191B2B.

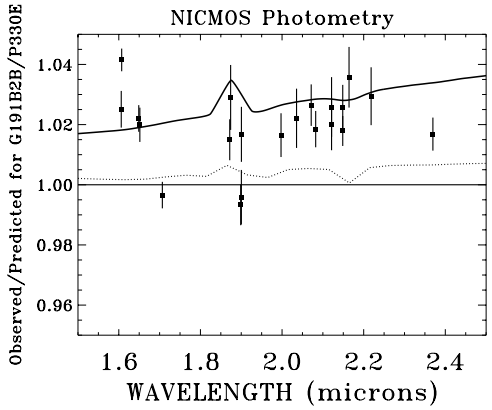

Figure 8. The data points with error bars are the observed NICMOS count rate ratios for G191B2B/P330E divided by the ratio of the standard star fluxes, using the old LTE model for G191B2B. The systematic trend for the data points to lie above unity means that either the standard model for G191B2B is too faint or the IR spectrum of the solar analog P330E is too bright. The heavy solid line is the change in the predicted ratio of the stellar observations based on the new NLTE model for G191B2B. The NLTE model predicts a ratio in better agreement with the bulk of the observations. The dotted line illustrates the minor difference between the new LTE models of Hubeny and the old LTE Koester standard.

4. Can Relative Fluxes Be Measured with a One Percent Accuracy?

4.1. Uncertainties in the Observations

The STIS observational uncertainties are dominated by the repeatability of observations of the same non-variable star and by uncertainty in the correction for CTE losses in the CCD modes, as long as the counting statistical uncertainty is negligible.

Repeatability: After fitting the changes in sensitivity as a function of time and wavelength, the residuals measure the lack of perfect repeatability for the 57 FUV and 59 NUV monitoring observations of GRW+70D5824 with the MAMAs and for the 31–35 observations of AGK+81D266 with the CCD. The repeatability depends on wavelength and on the bandpass bin size as summarized in Table 1. Some of the narrower bins have a comparable or better repeatability than the broad bands. Therefore, the correlation length for the fluctuations must be rather long, because the scatter does not "average out" with broader binning in wavelength. The observed narrower bandpass repeatabilities are corrected for the small effects of counting statistics and contribute to the modeled uncertainty as a linear interpolation between the measured wavelengths.

Table 1. Repeatability in broad bands.

MODE	Bandpass (Å)	one sigma (%)
G140L	350	0.54
	50	0.46–.79[a]
G230L	1000	0.18
	100	0.19–.59[a]
G230LB	1000	0.27
	100	0.27–.39[a]
G430L	2000	0.32
	200	0.20–.56[a]
G750L	2800	0.15
	400	0.13–.91[a]

[a] A small correction has been made for the contribution from counting statistics.

CTE Correction: Figure 9 shows some measured errors in the CTE correction and a fit to these points as a function of the number of electrons in the 7 pixel high standard extraction. This uncertainty affects the three low dispersion modes that utilize the CCD detector.

4.2. Uncertainties in the Model Flux Distributions

The formal uncertainty of ~ 1000 K in the $T_{\rm eff}$ determined from the Balmer line fits implies an uncertainty in the model fluxes relative to the V band of much less than 1%. In practice after normalizing the four models to their V magnitudes, there is as much as 1% scatter in the relative measured vs. model fluxes at 2000 Å and below. The agreement of the flux distributions from the two independent LTE codes is excellent below 1 μ, as illustrated in Figure 5. In the continuum, there are differences of 1% at the convergence of the Brackett lines around 1.6 μ for GD71 and at 3 μ for G191B2B, as shown in Figure 10. The NICMOS observations of G191B2B vs. P330E in Figure 8 support an uncertainty of $\sim$ 1% for the

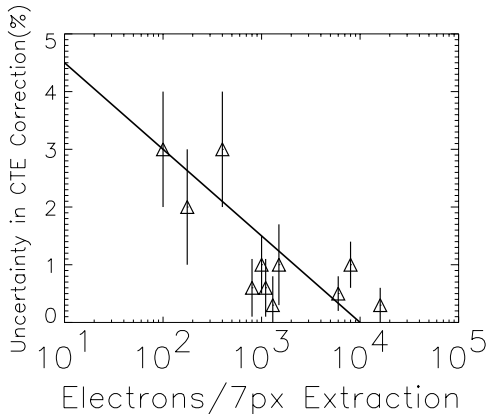

Figure 9. Measured errors in the CTE correction for various cases (triangles with error bars). The solid line is a fit to these data points and is used to model uncertainties in observed CCD spectrophotometry as a function of signal strength in electrons for point sources.

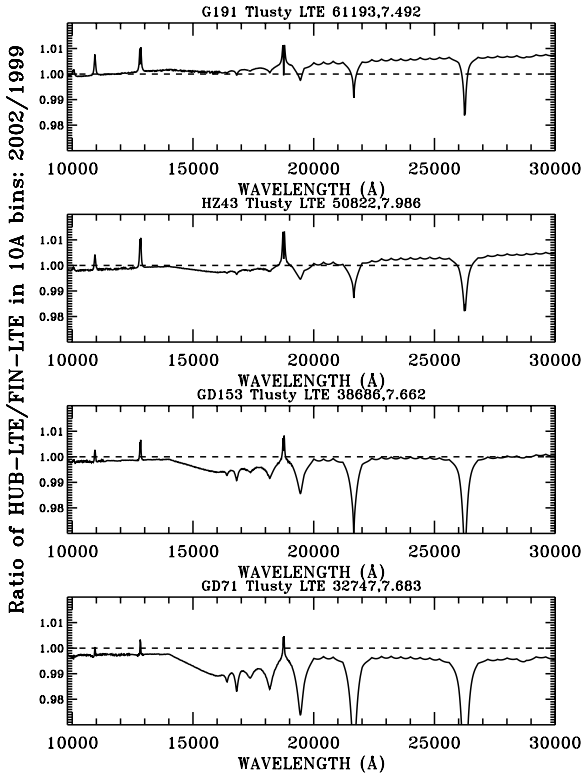

Figure 10. As in Figure 5 for the 1–3 μ region. The big dips at the locations of the B-β, B-δ, and B-γ are caused by the omission of these features in the old Koester models. In the continuum, differences between these LTE calculations approach $\sim 1\%$ around 1.6 μ for GD71 and at 3 μ for G191B2B.

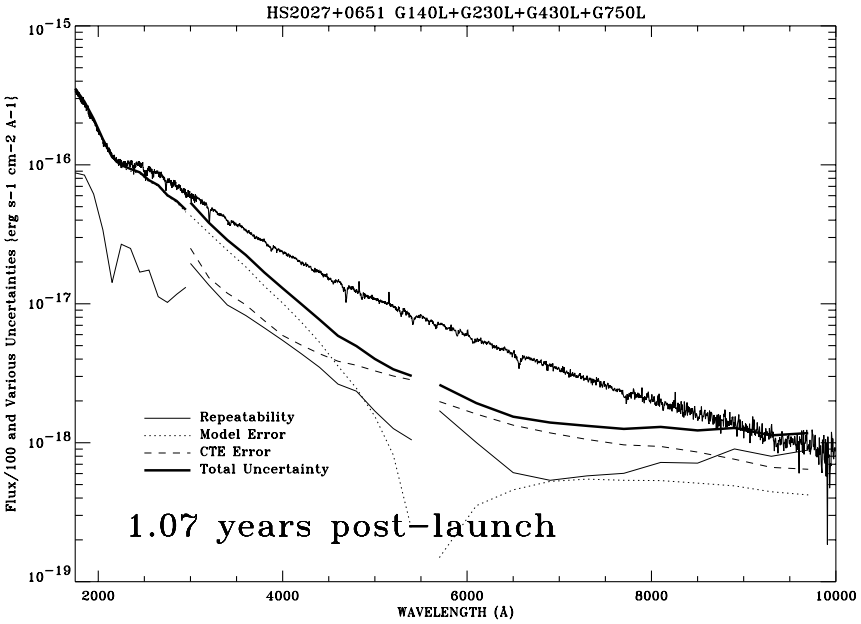

Figure 11. One percent of the stellar flux for HS2027+0651 (squiggly line), the total uncertainty relative to V (heavy smooth solid lines), and the three main components of the total uncertainty (light lines): repeatability (solid), model flux distribution (dotted), and the CTE correction (dashed). The total uncertainty for these data obtained about a year after launch exceeds 1% of the flux beyond 9300 Å, mainly because of poor repeatability combined with some CTE uncertainty.

adopted NLTE models beyond 1.5 μ. In summary, the model for the uncertainty in the STIS sensitivity and in measured secondary flux standards due to possible errors in the adopted flux distributions of the four prime standards is 1% below 2000 Å, decreasing linearly to zero in the normalization region at 5500 Å, and increasing to 1% at 1.5 μ and beyond.

4.3. Achieved Uncertainties for Secondary Standards

Figures 11–13 are examples of measured flux distributions and their uncertainties. The 2% grey uncertainty from the absolute flux uncertainty of Vega at V is not included; and a wavelength bin size sufficient to make the counting statistical error $\ll 1\%$ (i.e. $\gg 10,000$ counts) is assumed. One percent of the measured flux is plotted and compared to the component and total uncertainties. For the faint standard HS2027+0651 in Figure 11, the observations were obtained early in the mission, so that the CTE error (dashed line) is minimal and the total uncertainty (heavy solid line) exceeds 1% of the flux only beyond 9300 Å. Figure 12 is for another faint standard LDS749B obtained about five years post-launch, where the larger uncertainty in the CTE correction causes $> 1\%$ uncertainty at the short wavelength end of G430L at 3000–3300 Å and at the long wavelength end of G750L beyond 8600 Å. Because the repeatability error (thin solid line) is assumed to scale as the square root of the number of co-added observations, the repeatability error for the single G230L observation of LDS749B at 1900 Å is twice as large in % as for the co-addition of four spectra of HS2027+0651. In Figure 13, the recent single STIS observation of the bright Sloan standard BD+17D4708 with the three CCD modes has an uncertainty of $< 1\%$, except at wavelengths below 2100 Å, where this F star is faint.

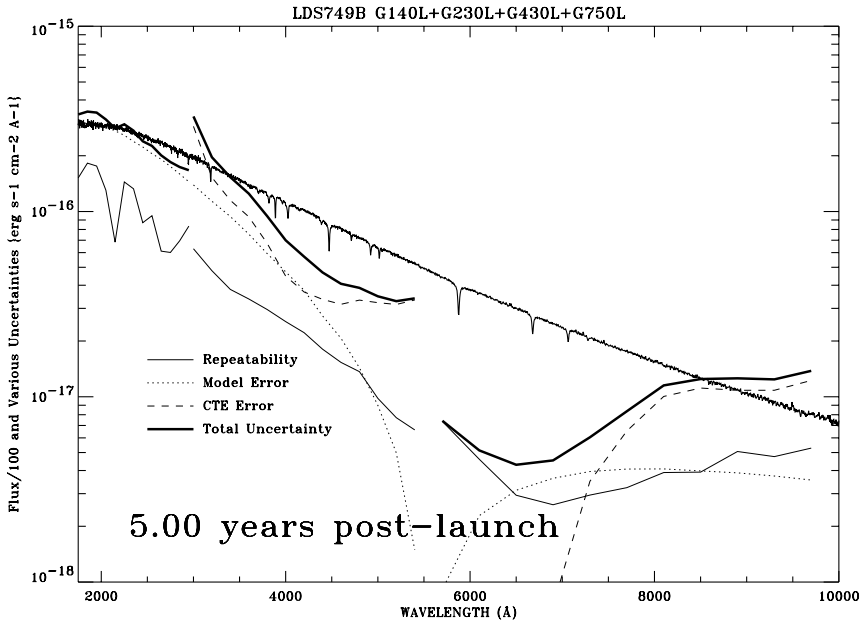

Figure 12. As in Figure 11 for LDS749B observed after five years of on-orbit radiation damage to the CCD. Uncertainty in the current preliminary CTE correction limits the precision in two regions of low sensitivity: 3000–3300 Å on G430L and beyond 8600 Å for G750L.

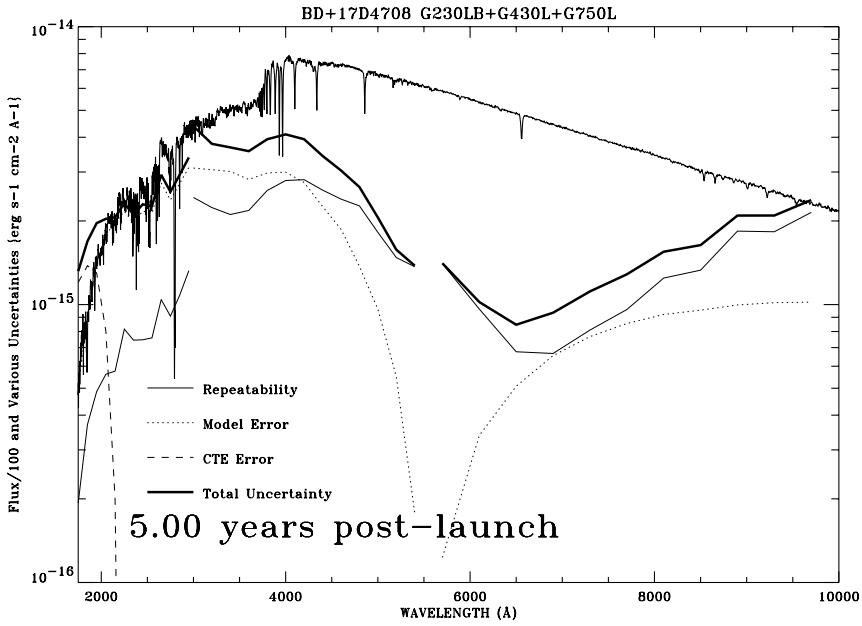

Figure 13. As in Figure 11 for the Sloan standard BD+17D4708. Only at the faint short wavelengths of G230LB do uncertainties of this bright (in the visible) secondary standard exceed one sigma = $\sim$ 1%. Only one recent observation has been utilized.

Can fluxes relative to V over the 0.1 to 3 μ region be determined to 1%? If the Balmer line profile analyses give the correct stellar temperature and gravities and the model atmosphere calculations correctly represent the physics, then the answer is yes, in some cases. The best flux distributions are measured for bright stars or early in the mission to avoid the uncertainties in correcting for CTE losses in the CCD detectors. (See the collection of *HST* standards at http://www.stsci.edu/instruments/observatory/cdbs/calspec.html.) At the longer wavelengths, the CCD fringing conspires with low sensitivity and large CTE losses to produce larger uncertainties. In summary, uncertainties as small as 1% can be achieved at some wavelengths, at some times, and for some ranges of stellar brightness. Don't forget that sigma here is only ONE sigma, not THREE and that the uncertainty in a comparison of two objects is the combination in quadrature of the sigmas of the separately measured fluxes.

References

Barstow, M. A., Holberg, J. B., Hubeny, I., Good, S. A., Levan, A. J., & Meru, F. 2001, MNRAS, 328, 211

Bohlin, R. 1999, *Instrument Science Report* STIS 99-07 (Baltimore: STScI)

Bohlin, R. C. 2000, AJ, 120, 437

Bohlin, R. 2002, *Instrument Science Report* STIS 02-xx (Baltimore: STScI) in preparation

Bohlin, R. C., Dickinson, M. E., and Calzetti, D. 2001, AJ, 122, 2118 (BDC)

Finley, D. S., Koester, D., & Basri, G. 1997, ApJ, 488, 375

Hayes, D. S. 1985, in Calibration of Fundamental Stellar Quantities, Proc. of IAU Symposium No. 111, ed. D. S. Hayes. L. E. Pasinetti, A. G. Davis Philip, (Reidel, Dordrecht), p. 225

Landolt, A. U. 1992, AJ, 104, 340

Stys, D., Walborn, N., & Sahu, K. 2002, *Instrument Science Report* STIS 2002-002 (Baltimore: STScI)